Endocardial infarct scar recognition by myocardial electrical impedance is not influenced by changes in cardiac activation sequence

Gerard Amorós-Figueras, MSc,* Esther Jorge, DVM, PhD,*† Concepción Alonso-Martin, MD, PhD,* Daniel Traver, MSc,‡ Maria Ballesta, BSc,§ Ramon Bragós, PhD,§ Javier Rosell-Ferrer, PhD,†§ Juan Cinca, MD, PhD*†

*From the *Department of Cardiology, Hospital de la Santa Creu i Sant Pau, IIB-Sant Pau, Universitat Autònoma de Barcelona, Barcelona, Spain, †CIBERCV, Barcelona, Spain, ‡Biosense Webster, Barcelona, Spain, and §Electronic and Biomedical Instrumentation Group, Department of Electronic Engineering, Universitat Politècnica de Catalunya, Barcelona, Spain.*

BACKGROUND Measurement of myocardial electrical impedance can allow recognition of infarct scar and is theoretically not influenced by changes in cardiac activation sequence, but this is not known.

OBJECTIVES The objectives of this study were to evaluate the ability of endocardial electrical impedance measurements to recognize areas of infarct scar and to assess the stability of the impedance data under changes in cardiac activation sequence.

METHODS One-month-old myocardial infarction confirmed by cardiac magnetic resonance imaging was induced in 5 pigs submitted to coronary artery catheter balloon occlusion. Electroanatomic data and local electrical impedance (magnitude, phase angle, and amplitude of the systolic-diastolic impedance curve) were recorded at multiple endocardial sites in sinus rhythm and during right ventricular pacing. By merging the cardiac magnetic resonance and electroanatomic data, we classified each impedance measurement site either as healthy (bipolar amplitude $\geq$1.5 mV and maximum pixel intensity $<$40%) or scar (bipolar amplitude $<$1.5 mV and maximum pixel intensity $\geq$40%).

RESULTS A total of 137 endocardial sites were studied. Compared to healthy tissue, areas of infarct scar showed 37.4% reduction in impedance magnitude ($P < .001$) and 21.5% decrease in phase angle ($P < .001$). The best predictive ability to detect infarct scar was achieved by the combination of the 4 impedance parameters (area under the receiver operating characteristic curve 0.96; 95% confidence interval 0.92–1.00). In contrast to voltage mapping, right ventricular pacing did not significantly modify the impedance data.

CONCLUSION Endocardial catheter measurement of electrical impedance can identify infarct scar regions, and in contrast to voltage mapping, the impedance data are not affected by changes in cardiac activation sequence.

KEYWORDS Electroanatomic mapping; Healed myocardial infarction; Myocardial electrical impedance; Pig; Ventricular pacing

(Heart Rhythm 2018;15:589–596)

Introduction

The clinical outcomes of catheter ablation in patients with infarct-related ventricular arrhythmias are largely dependent on the accurate delineation of the infarct scar during the procedure. Identification of the infarcted region is currently guided by 3-dimensional (3D) electroanatomic mapping, which use the voltage magnitude of local electrograms as a reference criterion.[1] Location of the dense infarcted region by bipolar voltage mapping has been correlated with anatomopathological and cardiac magnetic resonance (CMR) studies; thus, a low voltage threshold of $<$1.5 mV is currently accepted to delimit the borders of the infarct scar.[2,3]

A potential limitation of voltage mapping is that the amplitude of local electrograms may vary depending on the direction of the activation wavefront. Therefore, the collected data can change according to the type of the instantaneous cardiac rhythm. Indeed, significant differences in the amplitude of bipolar and unipolar local electrograms have been observed when the intrinsic rhythm is replaced by ventricular pacing in patients undergoing ablation of scar-related arrhythmias.[4,5]

Myocardial electrical impedance is a biophysical property of the heart that is influenced by the intrinsic structural

The first 2 authors contributed equally to this work. This work was supported by Fundació "La Marató de TV3" (grant no. 20150830), Spanish Ministerio de Economía y Competitividad, Instituto de Salud Carlos III (grant nos. FIS-PI13/00765 and DTS-15/00099), and Fondo Europeo de Desarrollo Regional (FEDER). Mr Traver is an employee of Biosense Webster. **Address reprint requests and correspondence:** Dr Esther Jorge, Department of Cardiology, Hospital de la Santa Creu i Sant Pau, c/Sant Antoni Mª Claret, 167, 08025 Barcelona, Spain. E-mail address: ejorge@santpau.cat.

1547-5271/

https://doi.org/10.1016/j.hrthm.2017.11.031

characteristics of the tissue.[6] Previous studies revealed that electrical impedance is lower in the infarct scar than in the normal myocardium, and this allows the recognition of the necrotic region.[7–9] Since electrical impedance is a passive property of the myocardium, it is predictable that impedance measures will not be affected by abrupt changes in cardiac activation sequence.

This study aimed to assess the ability of local electrical impedance to recognize infarcted tissue using an endocardial catheter and, secondly, to analyze comparatively the effects of abrupt changes in cardiac activation sequence on local voltage and impedance measurements using a closed-chest swine model.

Methods

Study population

Female domestic swine (Landrace and Large White cross) weighing 36 ± 1 kg were submitted to 2 interventions.

The first intervention aimed to induce acute myocardial infarction by occluding the left anterior descending coronary artery during 150 minutes with a catheter balloon, followed by reperfusion, as previously described.[10] Animals were premedicated with midazolam 0.6 mg/kg and ketamine 12 mg/kg, and then they were submitted to general anesthesia with propofol 2–4 mg/kg and maintained with sevoflurane inhalation (2.5%–3.5%). Fentanyl (5 μg/kg) was administered for analgesia. A femoral artery was catheterized and a 7-F introducer was used to insert a 6-F hockey stick guiding catheter (Cordis, Miami, FL). Under fluoroscopic control, the catheter was advanced to the left anterior descending coronary artery and a catheter balloon (Cordis) was placed at the mid segment below the origin of the first diagonal branch.

One month after the first intervention, a CMR study was performed in all animals under general anesthesia and mechanical ventilation to confirm and characterize the infarct scar. The day after the CMR study, the animals were sedated and anesthetized as in the first intervention. A femoral vein and femoral artery were catheterized, and a pacing electrocatheter (Blazer, Boston Scientific Corporation, Natick, MA) and a mapping electrocatheter (NAVISTAR, Biosense Webster, Inc., Diamond Bar, CA) were advanced into the right ventricle (RV) and left ventricle (LV), respectively. The RV electrocatheter was connected to a temporary external pacemaker (Medtronic Inc., Minneapolis, MN). The LV catheter was connected to a CARTO XP system (Biosense Webster) to generate an electroanatomic map as well as to a custom-designed impedance recording system to measure myocardial electrical impedance.[11] A conventional electrocardiographic (ECG) lead signal was continuously recorded throughout the procedure.

Study variables

CMR

We used a 3T scanner (Achieva, Philips Medical Systems, Amsterdam, The Netherlands), and all images were obtained with ECG gating and ventilation holding. The CMR study permitted to assess LV wall motion, cardiac function, and infarct characterization by late gadolinium enhancement (LGE). LGE images were obtained 10 minutes after an intravenous injection of 0.1 mmol/kg gadolinium-based contrast agent (Gadopentetate dimeglumine, Magnevist, Berlex Laboratories Inc., Wayne, NJ) with a pixel resolution of 1.18 × 1.18 mm in-plane and a slice thickness of 5 mm, giving rise to ~20 slices covering the LV. Processing of the LGE-CMR data was performed using the 3D Slicer software.[12] Briefly, an experienced operator manually segmented the LV wall in all sequential short-axis slices from the LGE-CMR images to create a 3D volume model of the LV (Figure 1). Then, normal and infarcted tissues were visualized and classified according to a maximum pixel intensity (MPI) cutoff of 0.40 × MPI (normal <0.40 and infarcted >0.40).

LV electroanatomic mapping

Local unipolar and bipolar electrograms were recorded at multiple endocardial sites, and the voltage amplitude of the signals was used to create a 3D representation of the LV chamber, as in current clinical electrophysiological procedures (Figure 1).

LV myocardial electrical impedance

Tissue impedance is a passive property of the myocardium that encompasses the intra- and extracellular resistances and cell membrane capacitance. Tissue impedance has 2 components: the impedance magnitude and the phase angle. The magnitude quantifies the drop in voltage of a test current passing through the tissue, and the phase angle reflects the time shift of the exploring current wave caused by the intrinsic structural characteristics of the tissue.

We measured the tissue impedance by injecting alternating currents (1-ms duration and 1-mA peak amplitude) of 26 frequencies (ranging from 1 to 1000 kHz) between the distal catheter electrode and a precordial skin reference electrode (Dispersive pad, 3M Healthcare Ltd, Saint Paul, MN) placed in the anterior precordial region. The voltage induced by the injected current was measured between the same distal catheter electrode and a second skin reference electrode (ECG pad, 3M) placed in the left lateral precordial region. This electrode configuration aimed to reduce the potential influence of both the individual body anatomy and the skin electrode impedance on the measurements. Moreover, to overcome the effect of the electrocatheter design (ie, electrode size and irrigated vs nonirrigated), we measured the intrinsic impedance of the electrocatheter before the study and this value was thereafter subtracted from the impedance measurement recorded during the study. All impedance measurements were recorded continuously during the cardiac cycle and stored at intervals of 2 seconds. Although we analyzed the entire impedance spectra in all sites, we preferentially reported the data at 1, 41, 307, and 1000 kHz because we previously verified that these frequencies were highly discriminative.[10,13]

To characterize the curve of phasic impedance changes elicited during the cardiac cycle, we measured the amplitude

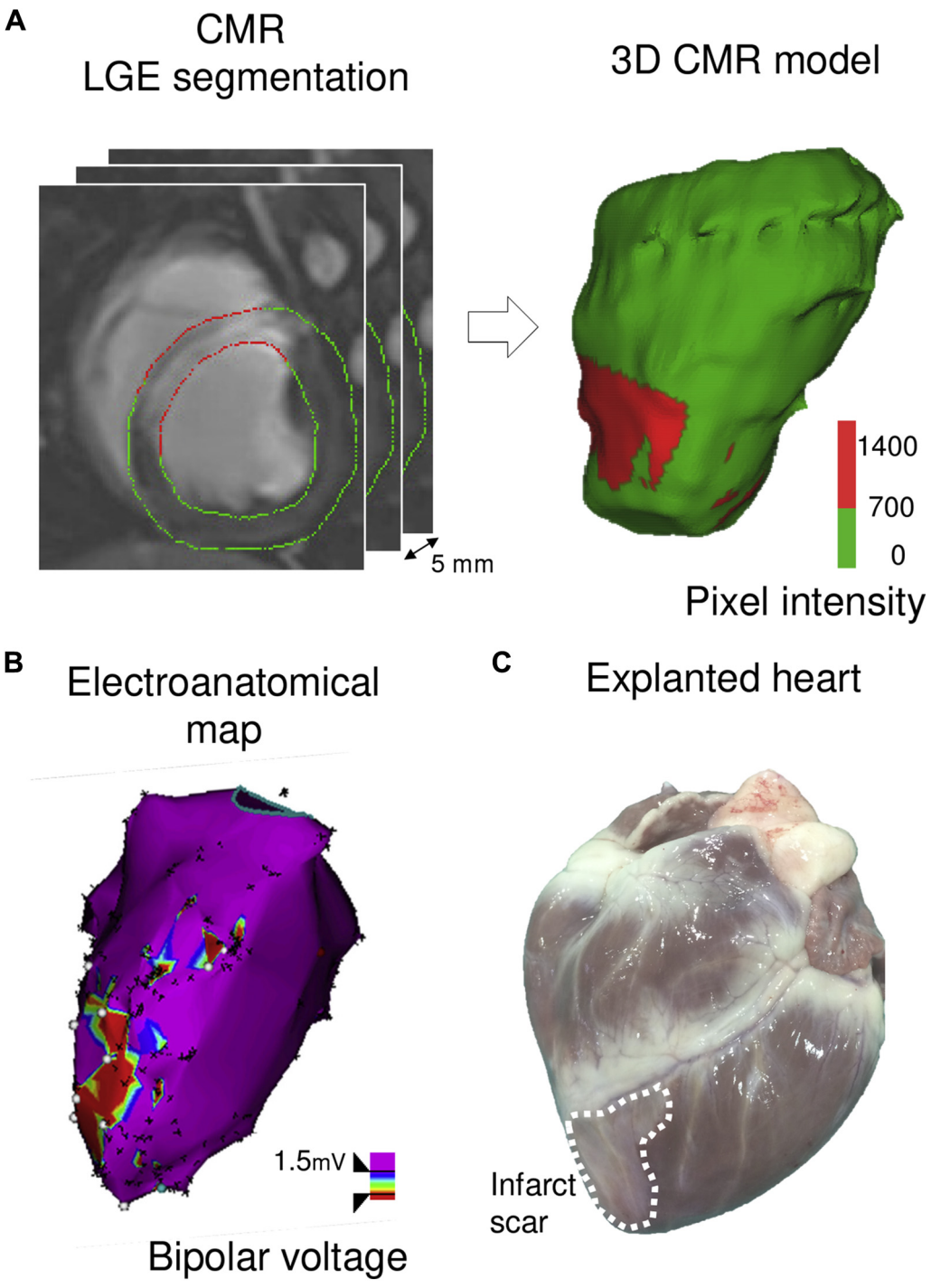

Figure 1 Illustration of the different imaging and electrophysiological techniques used in the study. **A:** Left: Myocardial wall segmentation in late gadolinium–enhanced cardiac magnetic resonance (LGE-CMR) imaging of a swine with a 1-month-old infarct scar. Right: Construction of a CMR model of the segmented slices. **B:** Electroanatomic map of the same case. **C**: Explanted heart of the same swine with the infarct scar borders delimited by a white dashed line.

of the curve and the time interval elapsed from the peak of the electrocardiographic R wave to the moment of maximum impedance magnitude (R wave impedance peak time).

CMR and electrical data merging

The electroanatomic data were automatically merged with the 3D CMR model using a fiducial registration guided by landmarks obtained in both techniques (LV apex and aortic and mitral annulus), as previously reported.[14] The areas of interest were defined on the basis of both the amplitude of bipolar electrograms and the extent of LGE on CMR imaging. Specifically, the measured sites were classified as healthy myocardium if they had a bipolar amplitude of $\geq$1.5 mV and an MPI of $<$40% or as infarct scar if they depicted a bipolar amplitude of $<$1.5 mV and an MPI of $\geq$40%. The sites not fulfilling this categorization were excluded.

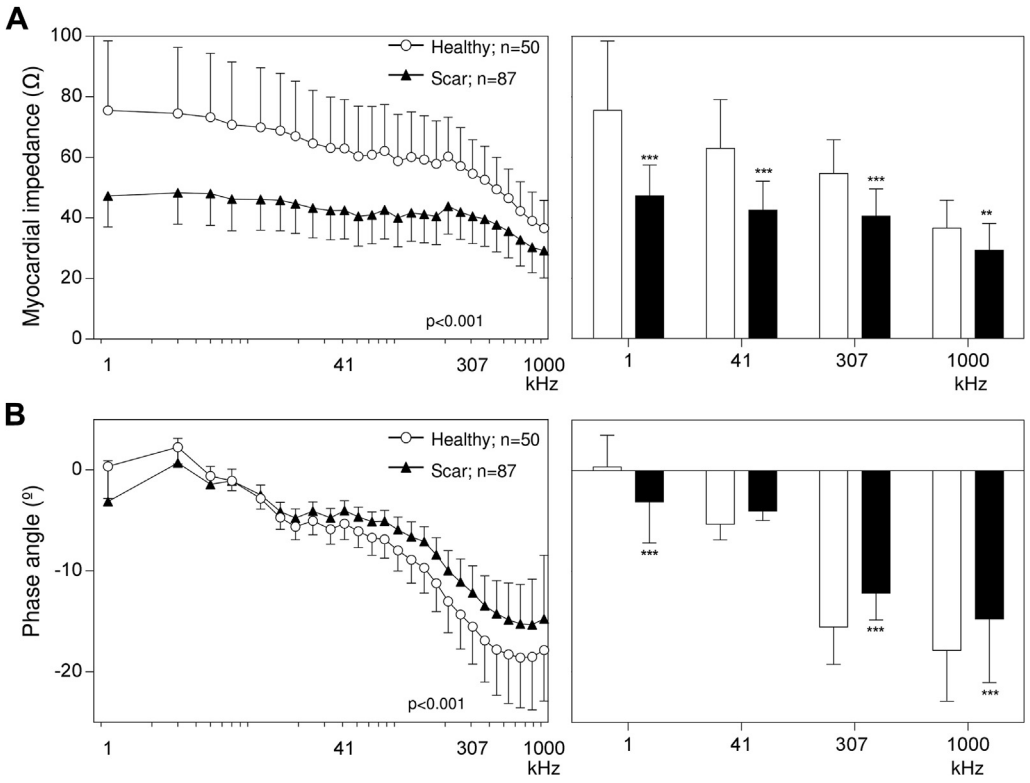

Figure 2 Mean values of the impedance magnitude and phase angle recorded in 137 endocardial sites (n = 50 healthy and n = 87 infarct scar) in 5 pigs. **A:** The left panel shows the mean of the impedance magnitude spectrum recorded in healthy and infarct scar sites. The right panel shows the mean of the impedance magnitude at 4 selected frequencies. **B:** The left panel shows the mean of the phase angle spectrum of healthy and infarct scar sites. The right panel shows the mean of the phase angle at 4 selected frequencies. $***P < .001$; $**P < .01$.

Changes in the cardiac activation sequence

To compare the stability of the electroanatomic data and the tissue impedance data under abrupt changes in the cardiac activation wavefront, these parameters were analyzed in the same sites during sinus rhythm and during electrical RV stimulation in a subset of measures. The resultant changes were expressed as percentages using the following formula: $100 \times [(X_{RVP} - X_{SR})/X_{SR}]$, where X_{RVP} are the values of voltage or impedance during RV pacing and X_{SR} are the values of voltage or impedance in sinus rhythm.

Experimental protocol

After stabilization of the level of anesthesia and hemodynamic parameters, an endocardial high-density 3D electroanatomic bipolar voltage map of the LV was constructed during stable sinus rhythm using the mapping catheter and the CARTO XP system. Thereafter, the mapping catheter was moved to different endocardial sites, and the local voltage and myocardial electrical impedance were measured at the same sites. In a subgroup of these sites, the local voltage and myocardial electrical impedance were recorded both in sinus rhythm and during RV pacing. At the end of the study, the animals were euthanized by an intravenous overdose of KCl and the hearts were explanted.

The study protocol was approved by the Animal Care and Use Committee of our institution and conformed to the *Guide for the Care and Use of Laboratory Animals*, 8th edition (National Research Council, The National Academies Press, Washington, DC, 2010).

Statistical analysis

Data were expressed as mean ± SD. Differences in the study variables were assessed using an analysis of variance with Bonferroni correction for post hoc comparisons. A binary logistic regression model was built to assess the influence of different impedance parameters to distinguish between normal and infarcted tissues. The discriminating power of the models was assessed using the receiver operating characteristic curve (ROC) and the area under the curve (AUC). Optimal cutoffs and accuracies were calculated for each impedance parameter model. The *P* value for the AUC comparison was based on the DeLong method. A *P* value of $<.05$ was considered statistically significant. Statistical analysis was performed using R version 3.2.2 (R Foundation for Statistical Computing, Vienna, Austria) and SPSS version 22.0 (IBM Corp., Armonk, NY).

Results

Two of the 7 (29%) pigs died during acute coronary occlusion due to irreversible ventricular fibrillation. The remaining 5 (71%) animals completed the entire protocol and were included in the final analysis. A total number of 156 sites were explored (27 ± 4 sites per animal). Nineteen (12%)

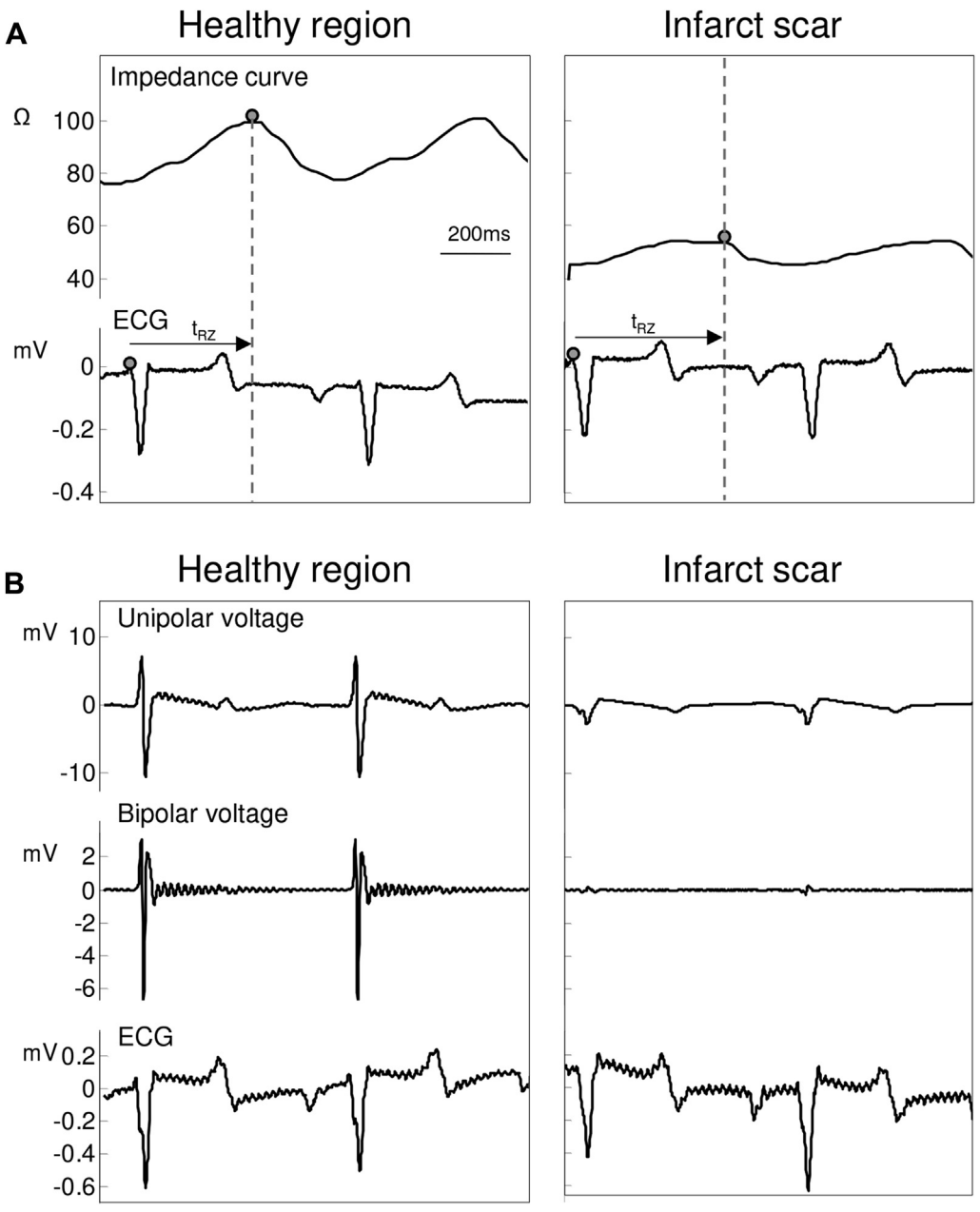

Figure 3 Myocardial impedance and voltage signals in healthy and scar tissues. **A:** Myocardial impedance curve and electrocardiographic (ECG) lead III recorded in healthy (left) and scar (right) regions in an anesthetized swine. The arrows indicate the time interval between the R-wave peak and the maximum of the myocardial impedance curve (t_{RZ}). **B:** Unipolar, bipolar, and ECG (lead III) signals at the site where impedance was measured in healthy (left) and scar (right) regions.

of these samples were excluded according to the categorization criteria; thus, 137 (88%) entered in the final analysis: 50 (36%) were classified as healthy and 87 (64%) as infarct scar.

Myocardial electrical impedance spectroscopy

As shown in Figure 2, the infarct scar showed lower electrical impedance magnitude and less negative phase angle than did healthy tissue (37.4% reduction in impedance magnitude at 1 kHz; $P < .001$ and 21.5% decrease in phase angle at 307 kHz; $P < .001$). The impedance magnitude (Z) decreased gradually at increasing current frequencies in normal tissue (from 75.5 ± 23.0 Ω at 1 kHz to 36.6 ± 9.2 Ω at 1000 kHz), but this change was less marked in scar tissue (from 47.3 ± 10.2 Ω at 1 kHz to 29.2 ± 9.0 Ω at 1000 kHz). Moreover, the phase angle spectrum showed a relaxation at high frequencies more apparent in healthy tissue than in scar tissue. Figure 2 shows that the excitation frequencies that best discriminate between healthy and scar tissues are 1, 41, and 307 kHz for the impedance magnitude and 1, 307, and 1000 kHz for the phase angle. All individuals showed a similar trend of changes in the impedance spectra in healthy and scar regions (Supplemental Figure 1).

Table 1 Values of the AUC-ROC and their optimal classification accuracy for the different myocardial electrical impedance parameters, either alone or in combination, measured at their most distinctive current frequency in 5 pigs with chronic myocardial infarction

Model	AUC-ROC (95% CI)	*P*	Optimal classification accuracy (%)
Impedance magnitude at 41 kHz	0.87 (0.81–0.94)	.001	79.8
Impedance phase angle at 307 kHz	0.78 (0.70–0.87)	.001	68.1
Impedance magnitude + phase angle	0.93 (0.87–0.99)	.001	93.3
Impedance curve (amplitude + peak time) at 41 kHz	0.93 (0.88–0.98)	.01	89.1
Combination of all impedance parameters	0.96 (0.92–1.00)	.001	93.3

AUC-ROC = area under the receiver operating characteristic curve; CI = confidence interval.

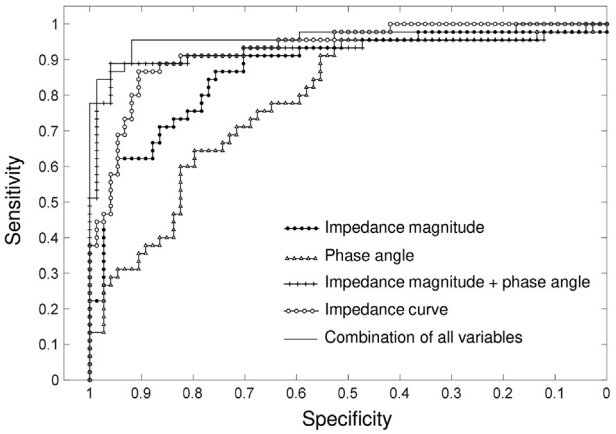

Figure 4 Receiver operating characteristic curves to assess the predictive ability of the different myocardial electrical impedance parameters. The impedance parameters used were (1) the impedance magnitude at 41 kHz (line with black circles), (2) the phase angle at 307 kHz (line with white triangles), (3) the combination of the impedance magnitude at 41 kHz and the phase angle at 307 kHz (line with plus markers), and (4) the combination of the amplitude of the impedance curve and the R wave-impedance peak time at 41 kHz (line with white circles). (5) The combination of all 4 impedance parameters (straight line).

Phasic pattern of myocardial electrical impedance

Myocardial impedance showed a biphasic pattern during the cardiac cycle. Figure 3 illustrates the relationship between the cyclic myocardial impedance changes and the ECG in healthy and scar regions. The amplitude of the phasic changes was lower in scar tissue at all tested current frequencies (13.5 ± 7.9 Ω vs 39.7 ± 15.6 Ω at 1 kHz, 10.3 ± 5.8 Ω vs 27.7 ± 10.7 Ω at 41 kHz, 8.9 ± 5.1 Ω vs 20.6 ± 9.9 Ω at 307 kHz, and 6.3 ± 3.8 Ω vs 11.6 ± 5.1 Ω at 1000 kHz; $P < .001$). The time interval between the R-wave peak of the ECG and the moment of the maximum value of the impedance curve was longer in scar areas than in the healthy myocardium (404 ± 102 ms vs 349 ± 115 ms; $P < .05$). The mean values of all impedance parameters recorded in each animal are presented in Supplemental Table 1.

Predictive ability of myocardial impedance

To assess the predictive ability of myocardial impedance measurement to discriminate between infarct scar and healthy tissue, we calculated the cutoff values and classification accuracy using the ROC curves (Table 1 and Figure 4). Cutoff values were 49.7 Ω for the impedance magnitude, −11.8° for the phase angle, 10 Ω for the amplitude of the impedance curve, and 394.5 ms for the R wave-impedance peak time. The inclusion of the 4 impedance parameters in the ROC model afforded the highest AUC, indicating optimal predictive ability ($P < .01$).

Effects of RV pacing on local voltage and tissue impedance

In 58 of the 137 (42%) explored sites, we analyzed the effects of RV pacing on both the amplitude of local electrograms and the magnitude of myocardial electrical impedance in each recording site. As shown in Figure 5A, RV pacing induced appreciable changes in the amplitude of bipolar and unipolar electrograms but not in the magnitude of myocardial impedance. The variability in these changes is graphically illustrated in Figure 5B, and their interquartile range values are reported in Table 2. Of note, in 12% (7) of the explored sites, the RV pacing entailed a switch on their bipolar threshold voltage classification: 8.6% (5) of sites changed from <1.5 mV in sinus rhythm to ≥1.5 mV during RV pacing and 3.4% (2) of sites from ≥1.5 to <1.5 mV. Likewise, unipolar electrograms followed a similar trend of changes in 10.4% (6) of the explored sites: 5.2% (3) changed from <8.3 mV in sinus rhythm to ≥8.3 mV during RV pacing and 5.2% (3) from ≥8.3 to <8.3 mV.

Discussion

Main findings

This study is the first to analyze the ability to recognize areas of infarct scar using a novel approach based on the endocardial catheter measurement of systolic-diastolic local myocardial electrical impedance. Our data indicate that the measurement of endocardial impedance allow the recognition of infarct scar and, as an advantage over the voltage mapping, the impedance data are not affected by abrupt changes in cardiac activation sequence.

Ability of myocardial impedance to identify infarcted tissue

Earlier experimental studies have demonstrated that the measurement of local myocardial electrical impedance permitted recognition of areas of acute and healed myocardial infarction by using either implanted transmural needle

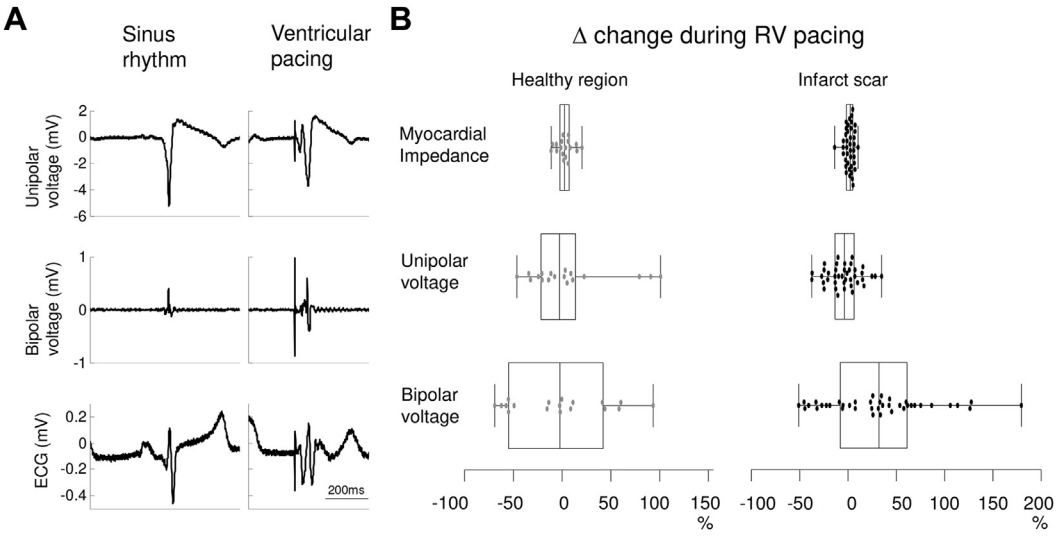

Figure 5 Effects of changes in cardiac activation sequence on local endocardial voltage and tissue electrical impedance. **A:** Unipolar and bipolar electrograms and electrocardiogram (lead III) recorded in sinus rhythm and during right ventricular (RV) pacing. **B:** Ratio of change (in percent) in myocardial impedance and endocardial voltage (unipolar and bipolar) induced by right ventricular pacing in healthy and infarct scar regions. The left side of the box plot represents the 25th percentile, and the right side represents the 75th percentile. The vertical line across the boxes represents the median value. The ends of the whiskers correspond to the lowest and highest values.

electrodes[7–9,15] or contact endocardial electrocatheters.[13,16] Most of these studies were conducted in open-chest models, and this limited the transferability of this technique to clinical practice. Moreover, myocardial impedance measurements could only be obtained at random moments within the cardiac cycle and this did not allow recording of the continuous changes induced by cardiac mechanical activity. More recently, with the use of fast broadband electrical impedance spectroscopy,[11] it has been possible to measure the impedance changes throughout the cardiac cycle using a wide range of current frequencies from 1 to 1000 kHz.[10,17] Using intramural needle electrodes, one of these studies[10] showed that the infarcted regions with greater fibrotic content had the lower mean impedance values and the more depressed systolic-diastolic impedance curve. The present data confirm that compared to the healthy myocardium, the impedance curve of the infarct scar has a reduced amplitude and a delayed peak value. The combined inclusion of the 4 impedance parameters (impedance magnitude, phase angle, amplitude of the impedance curve, and R wave-impedance peak time) into the ROC curve model increased the predictive ability and accuracy to differentiate healthy and infarcted tissues.

Effects of changes in cardiac activation sequence

Studies in patients submitted to catheter ablation of infarct-related ventricular arrhythmias have reported a voltage variability in local unipolar and bipolar electrograms when the intrinsic cardiac rhythm is replaced by ventricular pacing.[4,5] Specifically, these authors found that 8%–18% of the explored sites presented discordant voltage values during ventricular pacing (ie, sites with voltage amplitude <1.5 mV during 1 cardiac activation sequence changed to >1.5 mV during another activation sequence). Our results are consistent with these findings since we have found a similar pattern of voltage discordancy in 12% of the bipolar recording sites during RV pacing. Of note, the present study reveals that contrary to bipolar and unipolar voltage mapping, the measurements of myocardial electrical impedance in normal and infarcted regions were not modified by RV pacing. Thus, implementation of impedance measures in the 3D electroanatomic cardiac navigators would theoretically help assess more accurately the target infarcted areas, especially in the presence of recurrent ventricular arrhythmias during the procedure.

Table 2 Interquartile range values of the changes in local voltage and myocardial impedance induced by right ventricular pacing in 58 endocardial sites in 5 pigs with chronic myocardial infarction

Site	Unipolar voltage	Bipolar voltage	Impedance
Healthy (n = 18)	31.2%	87.2%	7.7%
Scar (n = 40)	18.4%	67.0%	6.4%

Study limitations

This study was designed to proof the concept that the impedance characteristics of the infarct scar can be detected by endocardial catheter mapping in closed-chest models and, secondly, to verify the lack of variability in impedance measures upon abrupt changes in cardiac activation sequence. At this stage, we divided the explored sites in only 2 well-defined categories (healthy or infarcted) taking as criterion standard both the bipolar voltage amplitude and the degree of gadolinium enhancement at each recording site (bipolar amplitude ≥ 1.5 mV and MPI $<40\%$ for healthy and bipolar amplitude <1.5 mV and MPI $>40\%$ for infarcted). Thus, to assess the diagnostic yielding of the impedance technique in nontransmural infarct sites, multisite recordings at the infarct border zone will be required.

Most of the commercial cardiac navigators can measure impedance parameters in order to check the appropriateness of electrode-tissue contact or to control the radiofrequency energy delivery during the ablation procedures. However, in contrast to our method, these systems do not permit continuous recording of the impedance during the cardiac cycle.

The present impedance data are specific for the mapping electrocatheter used in this study (Blazer), but other electrocatheter types can be used, provided a previous ad hoc in vitro impedance calibration will be performed.

Clinical implications

The transferability of our observations to the field of catheter ablation in patients with infarct-related ventricular arrhythmias is founded on (1) the cardiac electrophysiological similarities between humans and swine,[18] (2) the closed-chest approach in our study, (3) the use of electrocatheters and commercial 3D electroanatomic systems routinely used in clinical arrhythmia ablation, and (4) the use of the image merging process of CMR and electroanatomic data. Thus, our study suggests that the implementation of impedance mapping into current cardiac navigators will improve the identification of infarct scar targets.

Conclusion

Endocardial catheter measurement of tissue electrical impedance can identify infarct scar regions and, in contrast to voltage mapping, is not affected by changes in cardiac activation sequence.

Acknowledgments

We thank Francisco Alarcón, MSc, and David Soto-Iglesias, PhD for technical assistance.

Appendix

Supplementary data

Supplementary data associated with this article can be found in the online version at https://doi.org/10.1016/j.hrthm.2017.11.031.

References

1. Wissner E, Stevenson WG, Kuck KH. Catheter ablation of ventricular tachycardia in ischaemic and non-ischaemic cardiomyopathy: where are we today? A clinical review. Eur Heart J 2012;33:1440–1450.
2. Callans DJ, Ren JF, Michele J, Marchlinski FE, Dillon SM. Electroanatomic left ventricular mapping in the porcine model of healed anterior myocardial infarction: correlation with intracardiac echocardiography and pathological analysis. Circulation 1999;100:1744–1750.
3. Marchlinski FE, Callans DJ, Gottlieb CD, Zado E. Linear ablation lesions for control of unmappable ventricular tachycardia in patients with ischemic and nonischemic cardiomyopathy. Circulation 2000;101:1288–1296.
4. Tung R, Josephson ME, Bradfield JS, Shivkumar K. Directional influences of ventricular activation on myocardial scar characterization: voltage mapping with multiple wavefronts during ventricular tachycardia ablation. Circ Arrhythm Electrophysiol 2016;9:e004155.
5. Bruncklorst CB, Delacretaz E, Soejima K, Maisel WH, Friedman PL, Stevenson WG. Impact of changing activation sequence on bipolar electrogram amplitude for voltage mapping of left ventricular infarcts causing ventricular tachycardia. J Interv Card Electrophysiol 2005;12:137–141.
6. Sperelakis N, Hoshiko T. Electrical impedance of cardiac muscle. Circ Res 1961;9:1280–1283.
7. Cinca J, Warren M, Carreño A, Tresànchez M, Armadans L, Gómez P, Soler-Soler J. Changes in myocardial electrical impedance induced by coronary artery occlusion in pigs with and without preconditioning: correlation with local ST-segment potential and ventricular arrhythmias. Circulation 1997;96:3079–3086.
8. Cinca J, Warren M, Rodríguez-Sinovas A, Tresànchez M, Carreño A, Bragós R, Casas O, Domingo A, Soler-Soler J. Passive transmission of ischemic ST segment changes in low electrical resistance myocardial infarct scar in the pig. Cardiovasc Res 1998;40:103–112.
9. Schwartzman D, Chang I, Michele JJ, Mirotznik MS, Foster KR. Electrical impedance properties of normal and chronically infarcted left ventricular myocardium. J Interv Card Electrophysiol 1999;3:213–224.
10. Amorós-Figueras G, Jorge E, García-Sánchez T, Bragós R, Rosell-Ferrer J, Cinca J. Recognition of fibrotic infarct density by the pattern of local systolic-diastolic myocardial electrical impedance. Front Physiol 2016;7:389.
11. Sanchez B, Schoukens J, Bragos R, Vandersteen G. Novel estimation of the electrical bioimpedance using the local polynomial method: application to in vivo real-time myocardium tissue impedance characterization during the cardiac cycle. IEEE Trans Biomed Eng 2011;58:3376–3385.
12. Fedorov A, Beichel R, Kalpathy-Cramer J, et al. 3D Slicer as an image computing platform for the Quantitative Imaging Network. Magn Reson Imaging 2012;30:1323–1341.
13. Warren M, Bragós R, Casas O, Rodríguez-Sinovas A, Rosell J, Anivarro I, Cinca J. Percutaneous electrocatheter technique for on-line detection of healed transmural myocardial infarction. Pacing Clin Electrophysiol 2000;23:1283–1287.
14. Andreu D, Berruezo A, Ortiz-Pérez JT, Silva E, Mont L, Borràs R, De Caralt TM, Perea RJ, Fernández-Armenta J, Zeljko H, Brugada J. Integration of 3D electroanatomic maps and magnetic resonance scar characterization into the navigation system to guide ventricular tachycardia ablation. Circ Arrhythm Electrophysiol 2011;4:674–683.
15. Fallert MA, Mirotznik MS, Downing SW, Savage EB, Foster KR, Josephson ME, Bogen DK. Myocardial electrical impedance mapping of ischemic sheep hearts and healing aneurysms. Circulation 1993;87:199–207.
16. Wolf T, Gepstein L, Hayam G, Zaretzky A, Shofty R, Kirshenbaum D, Uretzky G, Oron U, Ben-haim SA. Three-dimensional endocardial impedance mapping: a new approach for myocardial infarction assessment. Am J Physiol Heart Circ Physiol 2001;280:H179–H188.
17. Jorge E, Amorós-Figueras G, García-Sánchez T, Bragós R, Rosell-Ferrer J, Cinca J. Early detection of acute transmural myocardial ischemia by the phasic systolic- diastolic changes of local tissue electrical impedance. Am J Physiol Heart Circ Physiol 2016;310:H436–H443.
18. Cinca J, Janse MJ, Moréna H, Candell J, Valle V, Durrer D. Mechanism and time course of the early electrical changes during acute coronary artery occlusion: an attempt to correlate the early ECG changes in man to the cellular electrophysiology in the pig. Chest 1980;77:499–505.